Tectonophysics xxx (2009) xxx–xxx

Contents lists available at ScienceDirect

Tectonophysics

journal homepage: www.elsevier.com/locate/tecto

Subsurface fault geometries and crustal extension in the eastern Basin and Range Province, western U.S.

M. Soledad Velasco *, Richard A. Bennett, Roy A. Johnson, Sigrún Hreinsdóttir

Dept. of Geosciences, University of Arizona, United States

ARTICLE INFO

Article history:
Received 13 June 2008
Received in revised form 10 December 2008
Accepted 18 May 2009
Available online xxxx

Keywords:
Wasatch fault
Listric normal faults
Reactivated detachment
Seismic reflection data
Geodetic measurements

ABSTRACT

We provide the first synthesis of seismic reflection data and active present-day crustal deformation for the greater Wasatch fault zone. We analyzed a number of previously unpublished seismic reflection lines, horizontal and vertical crustal velocities from continuous GPS, and surface geology to investigate the relationships between interseismic strain accumulation, subsurface fault geometry, and geologic slip rates on seismogenic faults across the eastern third of the northern Basin and Range Province. The seismic reflection data show recent activity along high-angle normal faults that become listric with depth and appear to sole into preexisting décollements, possibly reactivating them. We interpret these listric normal faults as reactivated Sevier-age structures that are connected at depth with a regionally extensive detachment horizon. These observations of subsurface structure are consistent with the mapped geology in areas that have experienced significant extension. We modeled the crustal deformation data using a buried dislocation source in a homogeneous elastic half space. The estimated model results include a low-angle dislocation (~8–20°) at a locking depth of ~7–10 km and slipping at 3.2 ± 0.2 mm/yr. Despite the model's relative simplicity, we find that the predicted location of the dislocation is consistent with the interpreted seismic reflection data, and suggests an active regionally extensive sub-horizontal surface in the eastern Basin and Range. This result may imply that this surface represents aseismic creep across a reactivated low-angle fault plane or the onset of ductile flow in the lower crust at or beneath the brittle–ductile transition zone under the present-day Basin and Range extensional regime. This result may also have implications for crustal rheology, and suggests that geodesy might, under some circumstances, serve as an appropriate tool for inferring deeper crustal structure.

Published by Elsevier B.V.

1. Introduction

Understanding subsurface fault geometries and their relationship with structures observed at the surface is important for understanding fault-system mechanics. While seismic reflection data can provide snap-shots of subsurface fault geometries, geodetic measurements of crustal motion can provide valuable constraints on the kinematics of continental crustal deformation, complementing geological maps, and geophysical images that can show subsurface structure.

Interpretation of geodetic measurements that represent interseismic strain accumulation is usually done by using crustal deformation models that relate two-dimensional surface strain rate associated with the locked seismogenic parts of fault zones to the ductile strain patterns at subseismogenic depth. However, these models do not directly constrain the slip rates on the locked parts of the faults (e.g., Savage et al., 1992; Vergne et al., 2001; Bennett et al., 2007), nor do they unequivocally constrain the deeper processes driving strain accumulation (e.g., Savage, 1990; Savage et al., 1999; Savage, 2000; Zatman, 2000). Understanding how accumulated elastic strain might be converted into permanent slip on upper crustal faults, which is critical to our understanding of fault mechanics and seismic hazards, depends critically on the true subsurface fault geometry and rheological structure, which are typically only poorly known.

Continental normal faults may provide one of the best opportunities to investigate the pattern of mid- to lower crustal strain and its relationship with upper crustal fault structure because the subsurface structure of the faults may be precisely imaged using geophysical techniques, primarily seismic reflection. Moreover, both the hanging wall and footwall are often sub-aerially exposed, allowing for detailed geological mapping and precise geodetic surveying. In this study, we jointly interpret new and independent seismic reflection lines, continuous GPS datasets, and geological constraints from the eastern third of the northern Basin and Range Province to investigate the possible relationships between upper and lower crustal strain.

2. Regional tectonic setting

The Basin and Range province is a vast region of alternating mountain ranges and sediment-filled depressions bounded by the Colorado Plateau to the east, and a diffuse strike-slip plate boundary to

* Corresponding author.
E-mail address: mvelasco@email.arizona.edu (M.S. Velasco).

0040-1951/$ – see front matter. Published by Elsevier B.V.
doi:10.1016/j.tecto.2009.05.010

the west (Fig. 1). It is characterized by thin crust (~30 km) (e.g., Gilbert and Sheehan, 2004) and relatively high topography, and has been interpreted to be the result of extension driven by gravitationally unstable over-thickened crust (e.g., Coney and Harms, 1984; Dickinson, 2002; DeCelles and Coogan, 2006). The eastern third of the northern Basin and Range, on which we focus our interest here, is seismically active, containing the Intermountain Seismic Belt (Smith and Sbar, 1974; Smith and Arabasz, 1991). The Wasatch fault defines the eastern boundary of the Basin and Range and represents the structural transition with the Colorado Plateau. This fault is currently active (e.g., Savage et al., 1992; Martinez et al., 1998; Chang et al., 2006) and appears to be segmented along strike (e.g., Schwartz and Coppersmith, 1984; Wheeler and Krystinik, 1992; McCalpin et al., 1994; McCalpin and Nelson, 2001). Seismic reflection profiling suggests that these distinct active segments at the surface appear to coalesce at depth into a main basal detachment, which also allows interaction with other normal faults to the west (e.g., Wilson and Presnell, 1992; Constenius, 1996). Many other mapped faults west of the Wasatch Front are also presently active (e.g., Caskey et al., 1996; Colman et al., 2002; Friedrich et al., 2003; Niemi et al., 2004), evident by their surface expressions and slip histories, however, these faults appear to accommodate a significantly smaller fraction of the total eastern Basin and Range slip budget than the Wasatch fault.

According to published Global Positioning System (GPS) results (e.g., Dixon et al., 2000; Bennett et al., 2003), the northern Basin and Range Province is accommodating nearly 25% of the ~50 mm/yr of relative horizontal motion between the Pacific and North America plates. The eastern Basin and Range, specifically, is currently experiencing ~3 mm/yr of tectonic extension over a ~350 km-wide region (Bennett et al., 2003; Friedrich et al., 2003; Niemi et al., 2004). Although most of its present-day deformation is concentrated at its eastern margin, the Basin and Range has been uniformly extended by up to 200% since the late Oligocene (Proffett, 1977; Hamilton, 1978; Wernicke et al., 1988; Jones et al., 1992) involving numerous normal faults. In some cases, this large-scale Cenozoic crustal extension has exhumed mid-crustal rocks from 10–20 km depth (Anderson, 1971; Armstrong, 1972; Wright and Troxel, 1973; Wernicke, 1981; Wernicke et al., 1988; Satarugsa and Johnson, 1998) along low-angle detachment faults that evolved into metamorphic core complexes (e.g., Davis and Coney, 1979; Crittenden et al., 1980; Spencer, 1984; Coney and Harms, 1984; Spencer and Chase, 1989). In other cases, normal faults are thought to be reactivated structures from the Sevier fold and thrust belt (e.g., Mohapatra et al., 1993; Constenius, 1996; Coogan and DeCelles, 1996; Mohapatra and Johnson, 1998; Constenius et al., 2003). The latter structures mostly involve high-angle normal faults, ~50–60°, that become listric at depth and could flatten to ~10–20° at depths as shallow as 4–6 km (Mohapatra and Johnson, 1998). In most cases, these structures are already low-angle above the brittle–ductile transition zone, which is ~8–12 km below the surface in the eastern Basin and Range (e.g., Stewart, 1978; Eaton, 1982; Smith and Bruhn, 1984), and may sole downward into a main detachment at even greater depths (e.g., Constenius, 1996).

A basement-involved upper crustal low-angle normal fault is imaged on the Consortium of Continental Reflection Profiling (COCORP) seismic line and other related seismic profiles across the Sevier Desert basin (Allmendinger et al., 1983). This detachment appears on the seismic profile Utah line 1 (Fig. 1) as a continuous event from close to the surface near the Canyon Range (west of the Wasatch fault), down to over 5 s in two-way travel time (12–15 km), with a dip of approximately 11° to the west (Von Tish et al., 1985). This geometry led to the interpretation that the detachment was a previous thrust that had been reactivated by Cenozoic extensional structures

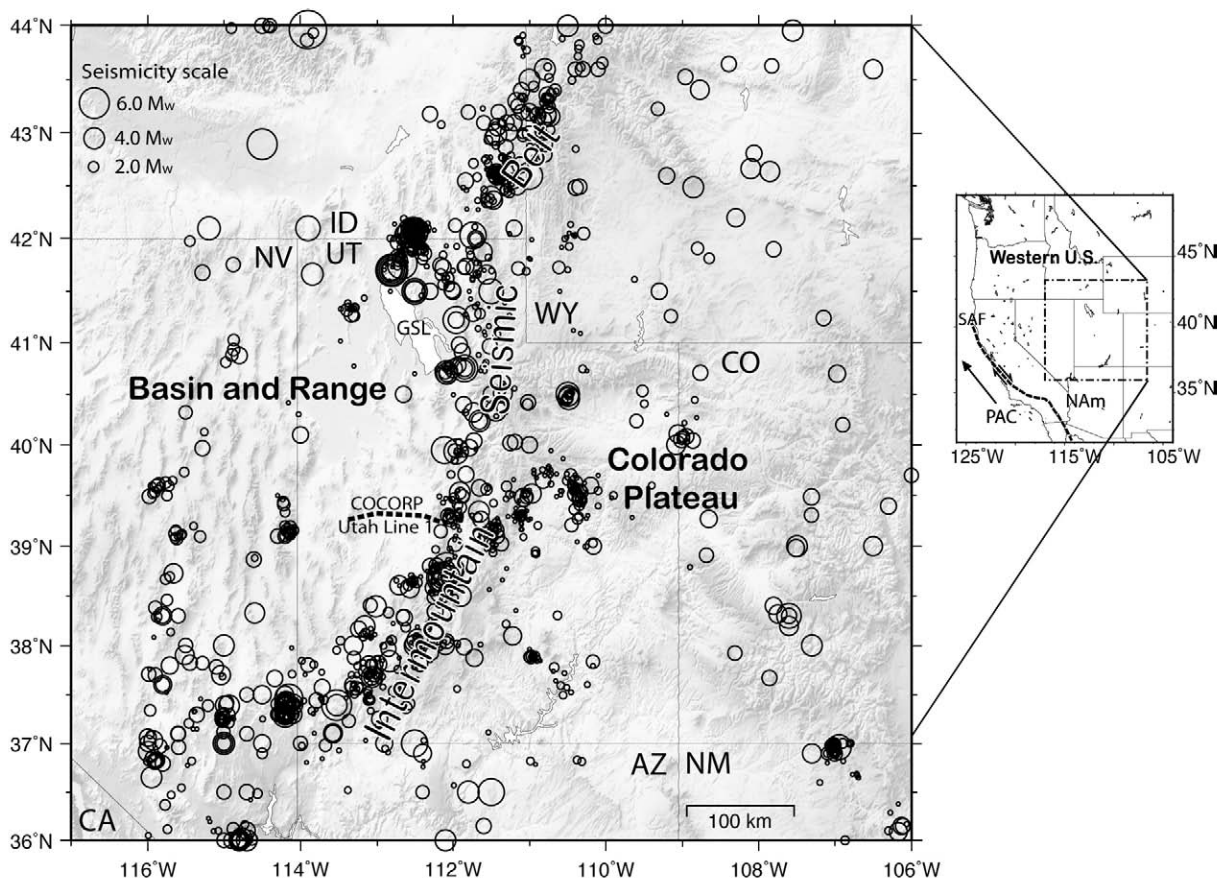

Fig. 1. Regional map of the western United States indicating area of study (right). Dashed line shows San Andreas Fault (SAF) and transform motion. Arrow shows motion of Pacific Plate (PAC) with respect to North American Plate (NAm). Regional map of the northern Basin and Range showing seismicity and location of COCORP Utah seismic line 1 (left).

Please cite this article as: Velasco, M.S., et al., Subsurface fault geometries and crustal extension in the eastern Basin and Range Province, western U.S., Tectonophysics (2009), doi:10.1016/j.tecto.2009.05.010

(e.g., Coogan and DeCelles, 1996). The western frontal fault of the Canyon Range at the eastern edge of the Sevier Desert basin has been suggested as the breakaway zone of the Sevier Desert detachment (Otton, 1995), although this interpretation has been challenged (e.g., Wills and Anders, 1996). Another interpretation was proposed by Anders and Christie-Blick (1994) based mainly on drill cuttings that revealed no microfractures near this fault surface. While high-density microfracturing near the contact is expected (Brock and Engelder, 1977), it was not found in samples within ~3 m of the Sevier Desert detachment surface. Therefore, Anders and Christie-Blick (1994) suggested that the reflection observed on the seismic line represents an unconformity rather than a low-angle normal fault.

Both geodetic and geologic data provide quantitative evidence for present-day Basin and Range extensional tectonics, although the time-scales represented by the different data types (structural geology, geomorphology, paleoseismology, geodesy) vary over disparate time-scales of 10 to 10^6 years (e.g., Wallace, 1987; Friedrich et al., 2003, 2004; Niemi et al., 2004). Discrepancies between rates inferred for the Wasatch fault zone using the spectrum of available methods have been interpreted as a possible indication of earthquake clustering (Niemi et al., 2004), transient postseismic strain associated with secondary faults west of the Wasatch fault (Friedrich et al., 2003), or persistent postseismic strain associated with the Wasatch fault (e.g., Malservisi et al., 2003). The available data appear to be incompatible with the traditional slip- or time-predictable models (Shimazaki and Nakata, 1980) for earthquake recurrence (Friedrich et al., 2003).

Not only have disparate time-scales from different data types led to diverse interpretations, but also varying fault geometry among different models has been discussed to explain geodetic measurements. While models using planar surfaces have been widely used to represent strain accumulation across the Wasatch fault to match geodetic data (e.g., Chang et al., 2006), others have shown that the observed extension on the hanging-wall block, normal to the strike of this fault, can also be explained by a listric geometry rather than planar (Savage et al., 1992; Bennett et al., 2007). Furthermore, a variety of dip angles have been suggested from earthquake focal mechanisms (e.g., Doser and Smith, 1989), surface expressions (e.g., McCalpin et al., 1994), and seismic reflection data (e.g., Smith and Bruhn, 1984), however there is still no clear understanding of the real subsurface geometry expected for this region (Table 1).

The eastern Basin and Range, as an active extensional environment, is an excellent place to investigate these uncertainties in slip rate, fault geometry, and nature of strain accumulation. In this paper, we concentrate on how elastic strain accumulating at depth relates to the fault structure in the brittle upper crust. If previous interpretations of fault geometries and active structures within the upper and middle crust are true, then present-day deformation should be reflected in the geodetic data. We, therefore, simultaneously combine independent results from seismic reflection data with both horizontal and vertical crustal motion measurements to investigate lower and upper crustal strain and their implications for the transition from ductile to brittle environments.

3. Seismic data analysis

We present seismic data from two profiles that image the subsurface geometries along different segments of the eastern Basin and Range (Fig. 2). The first profile is located along the Levan segment of the Wasatch fault and the second within the Great Salt Lake, in Utah. These vintage industry seismic lines were acquired in the late 1970s and early 1980s, and later donated to the University of Arizona.

The first profile (Fig. 3) is a collection of Exxon seismic lines, 84AU19, 85AH12 and 81J10, from west to east, respectively. Data from these seismic lines were processed by Exxon contractors using a standard seismic processing sequence and later donated as stacked profiles to the University of Arizona. We imported the stacked data files using workstation-based ProMAX interactive seismic data processing software (Landmark Graphics Inc.). We applied steep-dip finite-difference time migration and F–X deconvolution for signal enhancement and noise reduction to improve the seismic images. Finally, we depth converted these seismic lines with interval velocities calibrated to well-log information for easier display.

Fig. 3 shows the uninterpreted seismic sections above and our general interpretation below. The principal feature observed on Fig. 3 is a steeply west-dipping reflection surface that changes dip with depth and finally appears to sole into a low-angle interface at ~10 km. We interpret this reflection surface to represent a listric normal fault evidenced by its truncation of east-dipping reflections observed to the west. These east-dipping reflections could correspond to depositional surface or unconformities between the sedimentary rocks in the hanging wall. On the eastern part of this profile, close to the surface, we observe a steeply east-dipping reflection interface that also changes dip with depth. We also interpret this interface to represent a listric normal fault. Although it is harder to image, it is possible that this interface also soles into the same low-angle surface as the previously interpreted structure.

The shallow part of the interpreted listric normal fault to the west coincides with the surface trace of the Levan segment of the Wasatch fault. According to published seismic profiles and borehole data (e.g., Constenius et al., 2003; Horton et al., 2004), this fault appears to have cut through footwall Cretaceous–Eocene rocks at high angle, close to the surface, but Jurassic and Paleozoic rocks where the fault surface becomes listric, to finally sole into a low-angle surface, displacing Precambrian crystalline basement. The main structure to the east of the profile is interpreted to be the east-dipping Gunnison fault, which is also initiating at high angle, creating a small Tertiary–Quaternary fill

Table 1
Summary of Wasatch fault inferred dips and geometries obtained from different methods.

Wasatch Fault inferred dips[a]				
Technique	Geometry	Estimated dip	Depth	Study
Paleoseismology	Planar	68°–78°	Near-surface (<6 m)	McCalpin et al. (1994)
	Planar	60°–86°	Near-surface	Black et al. (1996)
	Planar	77°	Near-surface	Lund and Black (1998)
Earthquake Moment tensor	Planar	45°–60°	≥12 km	Doser and Smith (1989)
Reflection seismology	Listric	17° (N sections)	0.9 km	Smith and Bruhn (1984)
		6° (N sections)	1.3 km	
		34° (S sections)	1.9 km	
Geodetic data and related models	Planar	60°	Locking depth 15 km	Savage et al. (1992)
	Listric	60°	0–20 km	
		10°	Locking depth 20 km	
	Planar	26°–50°	Locking depth 17 km	Harris et al. (2000)
	Planar	55° (best fit)	Not reported	Chang et al. (2006)
	Planar	<~10°	Locking depth 10 km	Bennett et al. (2007)

[a] Only includes some studies exclusively pertaining the Wasatch Fault.

Please cite this article as: Velasco, M.S., et al., Subsurface fault geometries and crustal extension in the eastern Basin and Range Province, western U.S., Tectonophysics (2009), doi:10.1016/j.tecto.2009.05.010

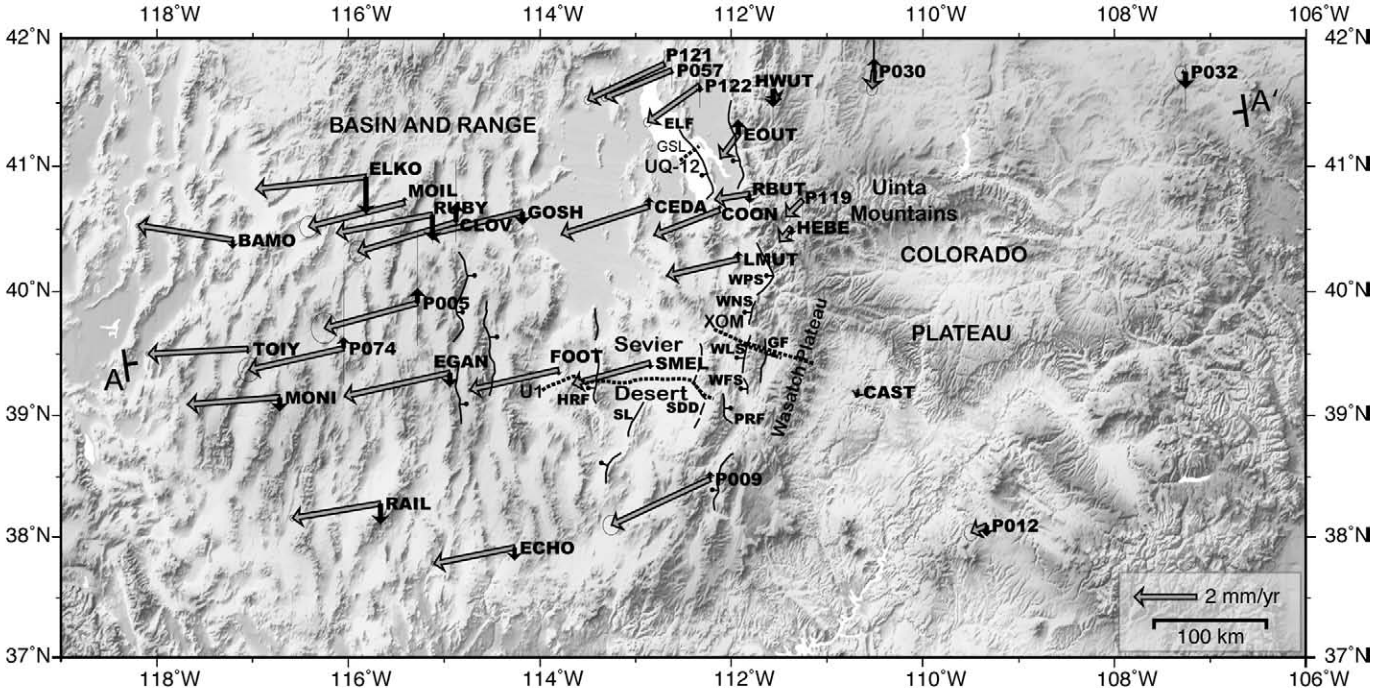

Fig. 2. GPS station map showing horizontal and vertical velocity fields estimated from continuous GPS measurements. Error ellipses represent the 95% confidence regions for the horizontal components. The error bars for the vertical rates represent 1*s* confidence level. All velocities refer to the Stable North America Reference Frame (SNARF) version 1.0. Main normal faults area shown in solid lines and seismic lines are shown in dashed lines (UQ-12; XOM: Exxon lines 84AU19, 85AH12, 81J10; U1: COCORP Utah Line 1). GSL: Great Salt Lake, ELF: East Lake Fault, WWS: Wasatch Weber Segment, WPS: Wasatch Provo Segment, WNS: Wasatch Nephi Segment, WLS: Wasatch Levan Segment, GF: Gunnison Fault, WFS: Wasatch Fayette Segment, PRF: Pavant Range Fault, SDD; Sevier Desert Detachment, SL: Sevier Lake, HRF: House Range Fault.

basin, chiefly displacing Cretaceous and early Tertiary rocks. At depth, this fault also becomes listric, principally gliding over Middle Jurassic deposits, and possibly soling into the same low-angle surface described above, but at higher levels within the stratigraphy (~6–8 km depth). These two normal faults create half-grabens, bounding the San Pitch Mountains and forming a triangle zone delimited at depth by a low-angle surface. According to Constenius et al. (2003), the deeper portions of these faults correspond to previous structures that, following the cessation of contractional deformation, collapsed during late Eocene–early Miocene time when the main basal thrust

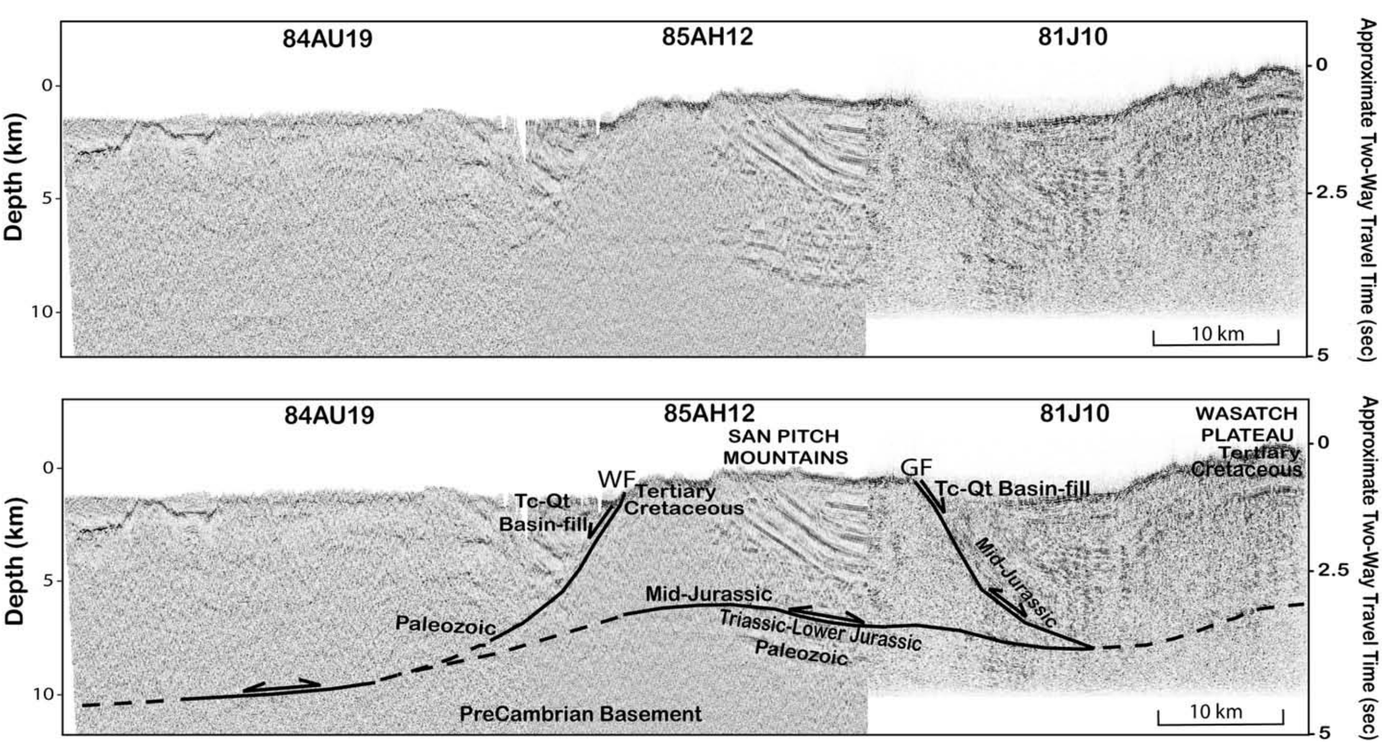

Fig. 3. Collage of depth converted seismic lines, from west to east of 84AU19, 85AH12 and 81J10. The uninterpreted sections are shown above and with interpretation below. WF: Wasatch Fault, GF: Gunnison Fault. Refer to figure for line location.

Please cite this article as: Velasco, M.S., et al., Subsurface fault geometries and crustal extension in the eastern Basin and Range Province, western U.S., Tectonophysics (2009), doi:10.1016/j.tecto.2009.05.010

was extensionally reactivated. Therefore, based on previously published studies (e.g., Constenius, 1996; Coogan and DeCelles, 1996; Constenius et al., 2003), we interpret these structures to be reactivated thrusts that appear to serve as gliding planes to the Cenozoic extensional regime that dominated the Great Basin.

The second section is located north of the previously shown seismic profile, within the Great Salt Lake (Fig. 4). The subsurface fault geometries beneath the Great Salt Lake were obtained from reprocessed seismic reflection lines collected by Amoco Production Company in the late 1970s. The original 24-channel data of Line UQ-12 (Fig. 4) were reprocessed at the University of Arizona using a standard seismic processing sequence (Mohapatra, 1996). Emphasis was given to optimization of the imaging of steep dips near fault planes through improved dip-moveout (DMO) algorithms. Additionally, we applied steep-dip finite-difference time migration, along with F–X deconvolution for signal enhancement and noise reduction, to improve the seismic images. Finally, we depth converted these data with interval velocities calibrated to well-log information.

One of the most prominent features of seismic reflection line UQ-12 (Fig. 4) is a steeply dipping reflection surface (~50–60°) that becomes shallower with depth. We interpret this reflection surface to be a high-angle normal fault near the surface that becomes listric at depth decreasing its angle to ~10–20° at ~4 km below the Great Salt Lake. Based on previously published seismic and borehole data (e.g., Mohapatra, 1996; Mohapatra and Johnson, 1998) this fault corresponds to the East Lake fault. This fault juxtaposes Tertiary basin-fill sediments against Precambrian and Lower Paleozoic basement, as well as a related antithetic (east-dipping) normal fault that soles into the main structure at depth. Both of these faults disrupt sub-horizontal reflections near the surface; however, above ~62 m the data quality becomes too poor to distinguish offset. Nevertheless, the observed structure suggests that these faults have very recent activity. According to Colman et al. (2002), the East Lake fault has been imaged to offset the lakebed and is thought to be active since the early Tertiary. Therefore, development of a fault scarp in a flat, shallow, internally drained basin, like the Great Salt Lake, indicates very recent fault activity along large faults beneath this region.

The profile in Fig. 4 also shows a low-angle reflection surface with spatially varying dip that, according to Mohapatra and Johnson (1998), appears to correspond to a thrust ramp to the east of the East Lake fault. This ramp is evidenced by truncated-east dipping layered reflections against it, and is thought to represent a preexisting structure inherited from the Sevier thrust belt (Mohapatra and Johnson, 1998). The wedge containing these folded units is bounded by the listric normal fault to the west and the low-angle fault to the east. If this interpretation is correct, then the East Lake fault is a normal fault that has reactivated previous structures at depth. Furthermore, according to Mohapatra and Johnson (1998), this thrust could represent a buried imbricate of the Willard thrust that is found exposed in the Ogden area along the Wasatch Front. The hanging wall of these outcrops contains a thin section of Precambrian metasedimentary and Paleozoic rocks, whereas the footwall exposes a thin section of Paleozoic overlaying Precambrian basement. These exposures are also observed at Antelope Island, within the Great Salt Lake (Mohapatra and Johnson, 1998).

At ~9 km depth, seismic line UQ-12 shows a strong sub-horizontal reflection, similar to those observed in the seismic lines shown in Fig. 3. Following our previous interpretation, this reflection could represent a low-angle surface into which the East Lake fault soles at depth, towards the west, out of the profile. Although not imaged in the seismic line, this low-angle surface could potentially correlate with the surface expression of the Weber segment of the Wasatch fault, located approximately 50 km to the east of this profile. Interpretation of additional seismic data within the Great Salt Lake (e.g., Mohapatra,

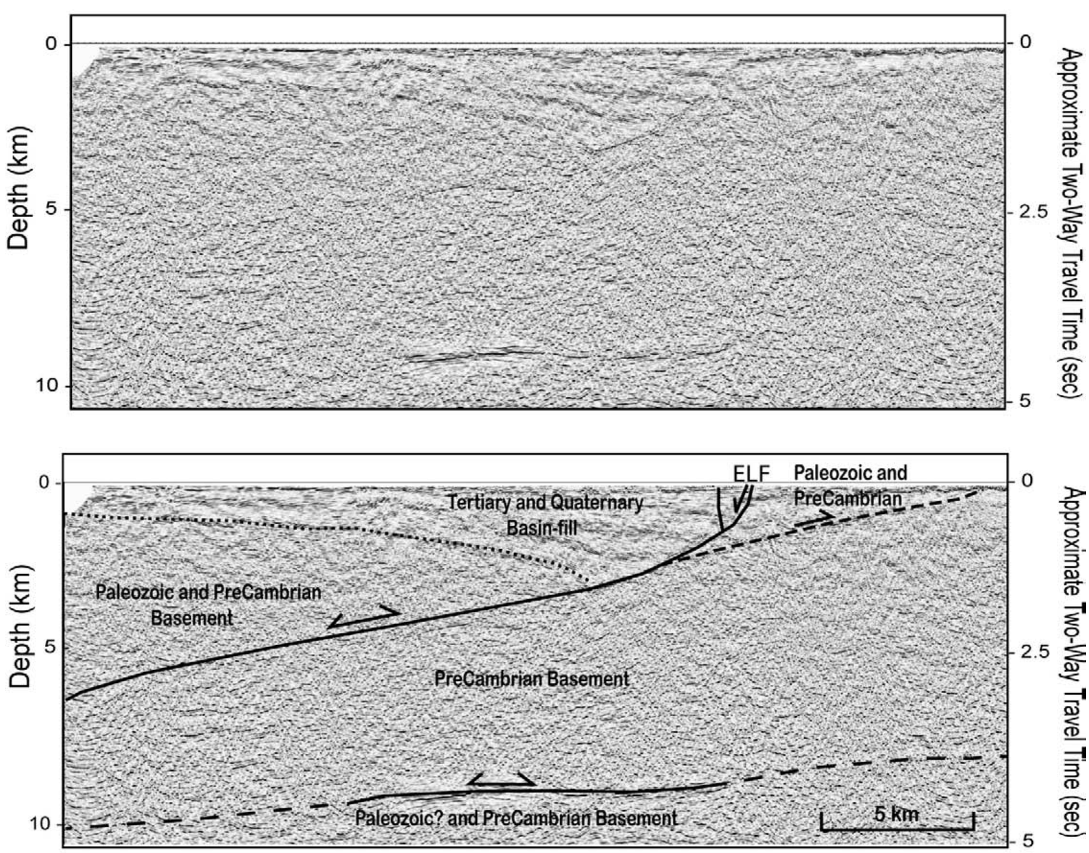

Fig. 4. Depth converted seismic line UQ-12, located within the Great Salt Lake. The uninterpreted section is shown above and with interpretation below. ELF: East Lake Fault. Refer to Fig. 3 for line location.

Please cite this article as: Velasco, M.S., et al., Subsurface fault geometries and crustal extension in the eastern Basin and Range Province, western U.S., Tectonophysics (2009), doi:10.1016/j.tecto.2009.05.010

1996; Mohapatra and Johnson, 1998) indicates that the Tertiary and Quaternary sediments were deposited in north-trending basins characterized by gently east-dipping beds over most of the west and central areas, in agreement with the interpretation of seismic line UQ-12 described above. In addition, these lines also show a major sub-horizontal reflection surface at depth, which appears to be an extensively continuous feature beneath the entire area.

Previously published geologic cross-sections and reconstructions along different latitudinal transects that traverse the Wasatch fault are consistent with the existence of low-angle structures that appear to be reactivated Sevier-age thrust surfaces, which have accommodated extensional collapse after the cessation of the Laramide orogeny (e.g., Mohapatra et al., 1993; Constenius, 1996, Coogan and DeCelles, 1996; Constenius et al., 2003). Based on our interpretations, we consider that the surface expressions of these high-angle normal faults reactivate preexisting thrust-fold structures and mechanically weak surfaces at depth, in agreement with the previously published geologic interpretations. We also believe that the sub-horizontal features observed consistently in all seismic profiles at 9–10 km depth, could represent a regionally extensive basal detachment that links at depth most normal faults observed at the surface. An alternative explanation for this low-angle surface could be that it represents a ductile shear zone. Published studies based on PASSCAL/COCORP data in the western U.S. (e.g., Holbrook et al., 1991) have suggested that strong reflections observed between 10 and 20 km depth could be the result of a ductile shearing mechanism at mid-crustal levels. Given the fact that the brittle–ductile transition in this area is found between 8 and 12 km (e.g., Stewart, 1978; Eaton, 1982; Smith and Bruhn, 1984), ductile shear zones could also explain the deeper low-angle surfaces observed on the presented seismic profiles. However, we find that portions of these low-angle surfaces are also observed at shallower depths (4–7 km), within the brittle upper crust, and therefore we find it compelling that in these cases, the low-angle surfaces observed correspond to reactivated Sevier-age structures. In particular, the distinct amplitude standout from the reflection observed at ~9 km depth in Fig. 4 represents a significant contrast that strongly suggests the existence of a detachment surface with a sliver of undeformed sedimentary rocks beneath this low-angle fault.

4. GPS data analysis

We analyzed data from 33 continuous GPS stations located in the eastern Basin and Range (Fig. 2) for the period from 1996 to 2008. The network covers a 1400-km-wide region across the greater Wasatch fault system. Our data analysis procedures were identical to those described in Bennett et al. (2007), but we here use a significantly larger data set that includes data from new stations belonging to the Plate Boundary Observatory (PBO) Facility network and other networks. The longest running stations, which form part of the PBO NUCLEUS array, have been in operation for approximately 12 years. We analyzed all existing data from these networks. All of these stations were established specifically for studies of crustal deformation and assessment of seismic hazards in the Wasatch region (e.g., Wernicke et al., 2004; Chang et al., 2006; http://pboweb.unavco.gov). We used the GAMIT software version 10.3 (Herring et al., 2006a) to analyze carrier phase data in 24-hour batches. We analyzed the 33-station eastern Basin and Range data set together with a select set of more than 200 stations distributed throughout North America and also different parts of the world in order to help define a stable reference frame. We used *a priori* orbits and Earth-orientation parameters from the International GNSS Service (IGS), but we estimated adjustments to these *a priori* parameters. The fundamental outputs of our GAMIT data reductions are site-position and Earth-orientation parameter estimates and associated error variance–covariance matrices. Changes in these parameters with time reveal motions of the Earth's surface. We used the forward Kalman filter capability of the GLOBK analysis software (Herring et al., 2006b) to estimate site velocities from the complete set of GAMIT results. We estimated temporally constant velocities for all sites simultaneously using all of the available variance–covariance information in order to exploit the precision of the network solutions, while at the same time insuring that all velocities share the same reference frame.

We determined velocity estimates relative to the Stable North America Reference Frame (SNARF) Version 1.0 (Blewitt et al., 2005). We realized this reference frame during our GLOBK analysis stage, by minimizing adjustments to SNARF at a set of core stations within the interior of the North America plate. We corrected for apparent site displacements associated with phase-center offsets related to radome and antenna changes. We did not estimate parameters representing periodic signals. Possible velocity bias related to annually repeating signals can be minimized by using sites that span greater than 2.5 years and almost eliminated by using a 4.5 year-span (Blewitt and Lavallee, 2002). Out of the 33 sites used in this study, 30 sites span greater than 2.5 years, whereas 26 span greater than 4.5 years. Thus, we expect that any velocity bias related to periodic signals should be negligible for 30 sites. The 3 sites having only 1.5 years of continuous data were excluded from the modeling.

The present-day horizontal and vertical velocity fields are shown in Fig. 2. The overall horizontal velocity field for the eastern Basin and Range suggests uniaxial east–west extension, with west components of motion generally increasing westward from the Colorado Plateau, and north components with constant slightly southward motion. Our results are in broad agreement with previously published data (Bennett et al., 1998; Thatcher et al., 1999; Bennett et al., 2003, Friedrich et al., 2003; Hammond and Thatcher, 2004; Niemi et al., 2004; Chang et al., 2006; Bennett et al., 2007), which show horizontal extension of ~3 mm/yr over an area of about 400 km in the eastern Basin and Range. The maximum horizontal velocity was found at EGAN, with 3.46 ± 0.01 mm/yr, located approximately 260 km west of the surface trace of the Wasatch fault.

Vertical velocities were estimated relative to SNARF (Fig. 2), giving rates that range between 0.3 and -1.2 mm/yr ($\sigma \leq 0.3$ mm/yr) with weighted average of -0.32 ± 0.15 mm/yr, in general agreement with previously published vertical results (Bennett et al., 2007). We determined a no-net-vertical (NNV) reference frame such that the weighted average vertical motion among the 33 stations used was zero, thereby mitigating any long wavelength velocity biases associated with global deformation processes and/or reference frame instability (Bennett et al., 2007). The measure of scatter, using the RMS vertical rates among the 33 sites, is 0.3 mm/yr, representing the combined effects of random measurement error, site-specific or short-wavelength systematic measurement error, and/or actual ground motion. The vertical signals for the Basin and Range might be associated with broad-scale gravitational collapse, elastic strain accumulation on one or more normal faults, viscoelastic relaxation following historic earthquakes, and/or non-tectonic signals such as those associated with volcanic centers, hydrological effects, and post-glacial isostatic rebound. The observed velocities show a slight longitudinal dependence; whereas sites in the east tend to move upward, sites to the west tend to move downward. By fitting a straight line to our observed dataset (Fig. 5), we obtain a constant velocity gradient with slope of 0.3 ± 0.4 nm/yr/km. The observed velocities relative to SNARF can be thought of as a combined effect of glacial isostatic adjustment (GIA), tectonics, and other deformation and noise processes (Bennett et al., 2007). The uncertainties associated with the GIA predicted by the SNARF model is ~0.5 mm/yr, which is for most sites higher than the estimated uncertainties of the observed GPS data. The calculated SNARF GIA model contribution to the stations used in this study is shown on Fig. 5 with a linear velocity gradient of -1.0 ± 0.4 nm/yr/km. The correction by subtracting the GIA effect to our observations would increase the gradient of the observed velocities by an amount of 1.2 ± 0.6 nm/yr/km (Fig. 5). Even though

Please cite this article as: Velasco, M.S., et al., Subsurface fault geometries and crustal extension in the eastern Basin and Range Province, western U.S., Tectonophysics (2009), doi:10.1016/j.tecto.2009.05.010

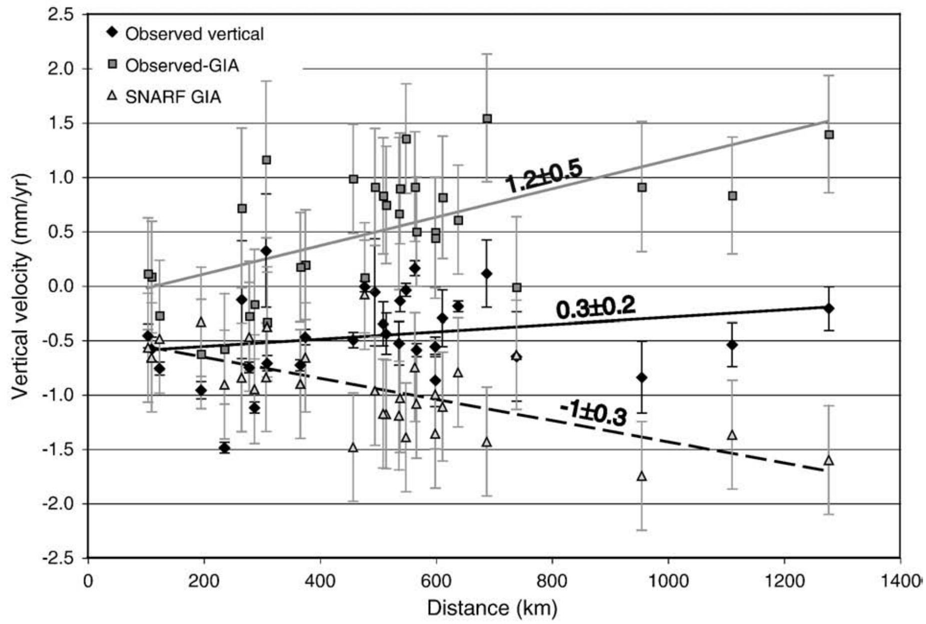

Fig. 5. Observed vertical rates relative to SNARF, SNARF GIA model evaluated at the GPS sites, and the observed minus SNARF rates (see text). Error bars represent 1σ for the observed, observed-GIA and SNARF GIA data points.

the GIA uncertainties are in most part larger than the uncertainties in the observed velocities, we find that the SNARF GIA model contribution may not be completely negligible. Therefore we utilize both the GIA-corrected and uncorrected GPS velocity estimates. Although we expect no significant contribution from correcting for the GIA, mainly due to its high uncertainty, we nevertheless explore its effects to our geodetically derived velocities for completeness.

4.1. Models

In order to explore the tectonic implications of the horizontal and vertical rate estimates, and their relationship to the upper crustal structure imaged by seismic reflection profiles as described above, we used a simple two-dimensional back-slip dislocation model in an elastic half space (Savage, 1983) to represent strain accumulation

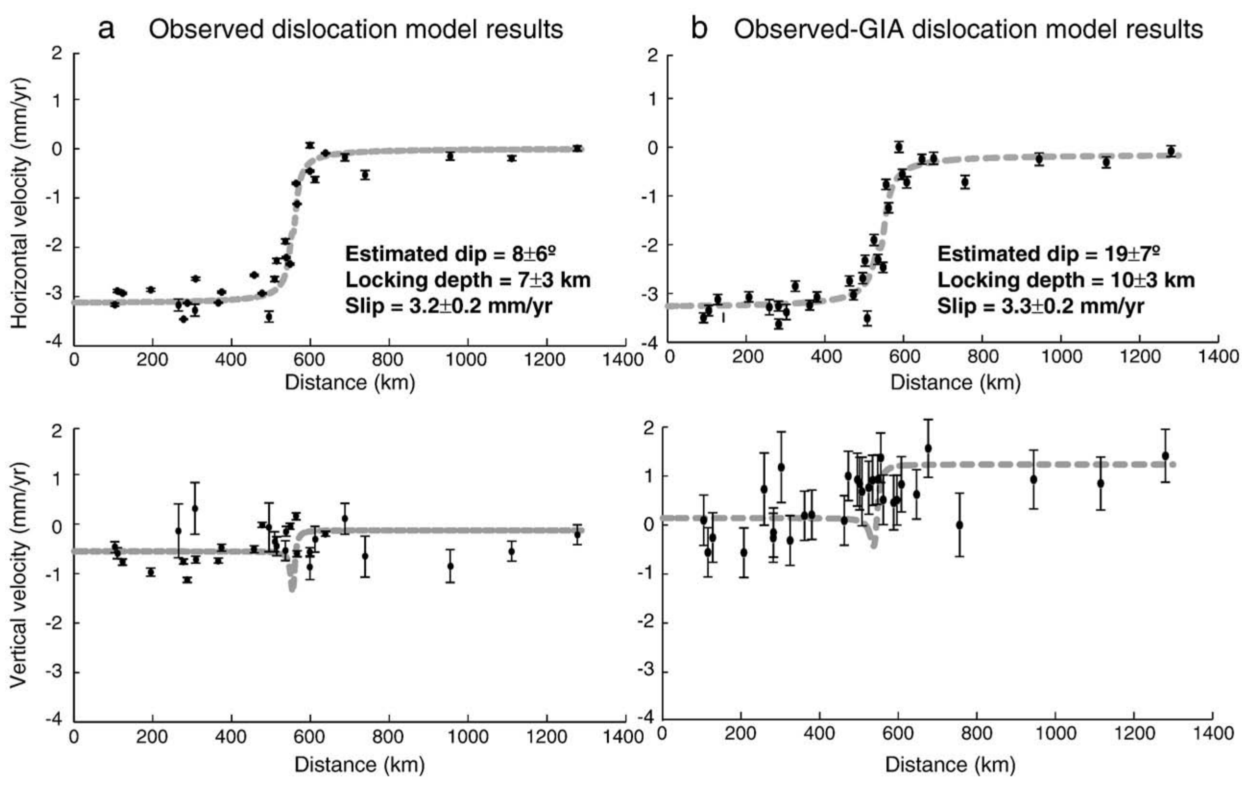

Fig. 6. Velocity profiles and elastic dislocation model results. The plots show measured horizontal (above) and vertical (below) velocities perpendicular to the strike of the Wasatch fault with 1σ, represented by the error bars. See A–A′ on Fig. 3 for profile location. These data were used to estimate a best-fit model for slip, dip locking depth and location on a normal fault. (a) Dislocation model results using the observed GPS dataset relative to SNARF. (b) Same as for (a) but showing dislocation model results using the observed-GIA model contribution.

Table 2
Range of values and model results obtained from the constrained random search algorithm used for predicting elastic dislocations.

Model parameters	Range of values	Model results
Observed		
Fault dip (°)	0–14	8 ± 6
Locking depth (km)	0–15	7 ± 3
Fault slip (mm/yr)	0–5	3.2 ± 0.2
Fault location (km)	0–1400	553 ± 5
Observed-GIA		
Fault dip (°)	0–30	19 ± 7
Locking depth (km)	0–20	10 ± 3
Fault slip (mm/yr)	0–5	3.3 ± 0.2
Fault location (km)	0–1400	553 ± 6

assuming one main buried dislocation (Fig. 6). We estimated dip, slip, locking depth, and location for a model of a west-dipping normal fault, using a constrained random search (CRS) algorithm (Brachetti et al., 1997). We used the vertical and horizontal velocity estimates from both the observed and the observed-GIA datasets, for sites located within a 1400 km long swath. The average azimuth of the horizontal components of site motion is N8°E, approximately orthogonal to the strike of the Wasatch fault (A–A′ of Fig. 2). We used the component of horizontal velocity projected onto this fault perpendicular direction. The RMS of the observed velocity component parallel to the fault plane is 0.3 ± 0.06 mm/yr, a factor of ~10 smaller than for the fault perpendicular components 2.4 ± 0.05 mm/yr. The RMS of the observed-GIA velocity component parallel to the fault plane is 0.5 ± 0.15 mm/yr, a factor of ~8 smaller than for the fault perpendicular components 2.5 ± 0.11 mm/yr. These values are indicating, that the GPS signal observed is very likely representing the extensional, perpendicular motion of the fault, confirming that our model is realistic. Furthermore, these values, along with the fact that the observed vectors east of this region have nearly zero horizontal velocity, are also indicating that the SNARF has been correctly determined and that it provides an appropriate frame of reference for our study. A best-fit fault model was obtained, for both GPS datasets (Fig. 6a and b), using the CRS algorithm by minimizing the χ^2 misfit of predicted velocities to the data. The ranges of values searched are listed in Table 2. We assessed the confidence regions and trade-offs among model fault parameter estimates using $\Delta\chi^2$ statistics (e.g., Press et al., 1986). Fig. 7a and b, shows the co-dependence of $\Delta\chi^2$ for select dislocation parameter pairs.

The best-fit fault dislocation for the observed dataset was found to have an estimated dip of 8 ± 6° at a locking depth of 7 ± 3 km (Fig. 6a). The horizontal location of the edge dislocation at depth lies just west of station RBUT. The amount of fault slip predicted by this model is 3.2 ± 0.2 mm/yr. The normalized RMS misfit of the best-fit model to the GPS data is 9.4. Although no systematic trend is apparent in the residuals to the model fit, the NRMS value greater than one could indicate that there are other signals that may need to be taken into account, e.g., GIA. It is also possible that a dislocation model is oversimplified, given the listric geometry observed in the seismic data. However, these model results are consistent with the low-angle nature of the surface observed in the seismic profile. Additionally, it is possible that the true deformation at the surface is more complicated; there could be other active faults that are ignored in this model or an overprinting signal that is not related to a geologic structure. The best-fit fault dislocation for the observed-GIA dataset was found to have an estimated dip of 19 ± 7° at a locking depth of 10 ± 3 km (Fig. 6b), and in agreement, within error, with the dislocation found by the previously mentioned model. The amount of fault slip predicted by this model is 3.3 ± 0.2 mm/yr. The normalized RMS misfit of the best-fit model to the GPS data is 2.3. This value is much lower than for the previous model results, mainly due to the higher uncertainties associated with the GIA.

Despite their simplicity, these model results are in accordance with the study of Bennett et al. (2007), which found that horizontal and vertical rates from continuous GPS in the vicinity of the Wasatch fault are inconsistent with slip on structures dipping greater than 30°. The locking depth that we estimated based on the CRS is, within uncertainty, consistent with a transition from stick-slip to stable sliding or ductile flow at the brittle–ductile transition zone in this region (8–12 km) (e.g., Stewart, 1978; Eaton, 1982; Smith and Bruhn, 1984).

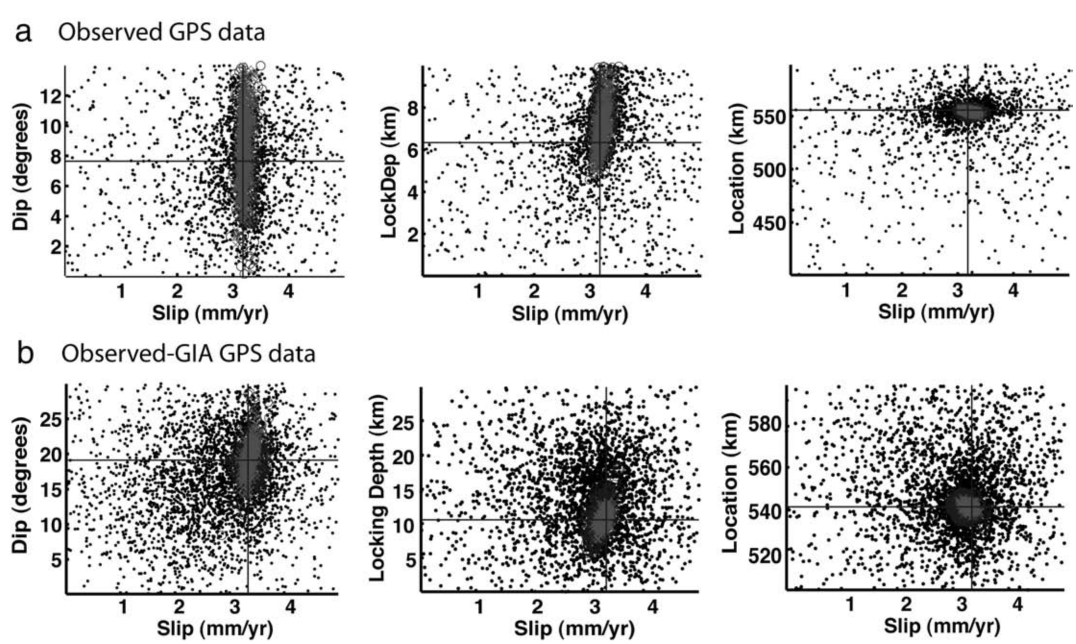

Fig. 7. Pair plots of the measure of the fit of the estimated parameters used in the dislocation models: (a) using the observed GPS data relative to SNARF and (b) using the observed-GIA model contribution.

5. Geodynamic implications and discussion

Based on our interpretation of seismic reflection and GPS data, we illustrate our results in two simplified cross-sections of the upper 15 km of the crust of the eastern Basin and Range (Fig. 8a and b). The schematic cross-section of Fig. 8a shows the rates and pattern of lower crustal strain inferred from the crustal deformation analysis, as well as the elastic dislocation model results derived from the observed and observed-GIA datasets. This figure also accounts for the listric and low-angle geometry of the Wasatch fault observed at depth, which was digitized from the seismic data. Despite the relative simplicity of the elastic dislocation model, we find that the predicted dislocations are in general agreement with the seismic reflection data, and consistent with a regionally extensive low-angle surface in the eastern Basin and Range. Furthermore, these results imply that this surface may represent aseismic creep across a low-angle normal fault plane or the onset of ductile flow in the lower crust beneath the brittle–ductile transition zone under the present-day Basin and Range extensional regime. We consider that most, if not all, surface expressions of normal faults observed in the seismic data presented here are linked at depth by reactivating previous thrusts that sole into this regionally extensive detachment (Fig. 8b). Based on our seismic interpretations, this detachment can vary between depths of 6 and 10 km, depending on where in the stratigraphic section the previous thrusts were located. Our interpretation is in agreement with previous studies carried out in the Sevier belt and Basin and Range areas (e.g., Constenius, 1996; Coogan and DeCelles, 1996).

Our analysis of seismic reflection data from Utah provides a better understanding of the geometries of upper crustal faults within the eastern Basin and Range. Our interpretations of seismic reflection data from beneath the Great Salt Lake and farther south in central Utah, across the Wasatch fault, show that the major basin-bounding normal faults, including the Wasatch fault, generally have a listric shape, becoming sub-horizontal at depths as shallow as 4 km, but no deeper than ~11 km. These faults also appear to offset the surface, showing recent activity; of these faults, the Wasatch fault is considered the most active. The rapid decrease in fault dip at depths shallower than the brittle–ductile transition zone in the Basin and Range might be explained by a gradual change of rheology and/or stress orientations with depth. However, immediately west of the Wasatch Front (beneath the Great Salt Lake), the Sevier-age Willard and related thrusts, form reactivated structures into which the Tertiary listric normal faults sole (Constenius, 1996; Mohapatra and Johnson, 1998). Similarly, the Sevier Desert detachment (Allmendinger et al., 1983) and related low-angle planar normal faults are not easily explained by mechanical fault theory (e.g., Scholz, 1990), which suggests that at least some control on their structural development is exerted by preexisting structures (e.g., Coogan and DeCelles, 1996) or geological anisotropy.

There has been a long-standing debate in the scientific community regarding mechanisms and geometries of continental extension, especially the role of low-angle normal faults in active tectonic settings (e.g., Wernicke, 1981). These low-angle structures are observed in the geologic record (e.g., Abers, 1991; Johnson and Loy, 1992; Wernicke, 1995) and in seismic reflection lines (e.g., COCORP Utah Line 1); however, Andersonian fault theory generally precludes slip on low-angle surfaces. Extending regions in the brittle upper crust are typically described by vertical principal stresses and Byerlee's law (Byerlee, 1978), and should be characterized by normal faults that initiate at ~60° (e.g., Sibson, 1985). Focal mechanisms for recorded normal events tend to be high angle, generally consistent with

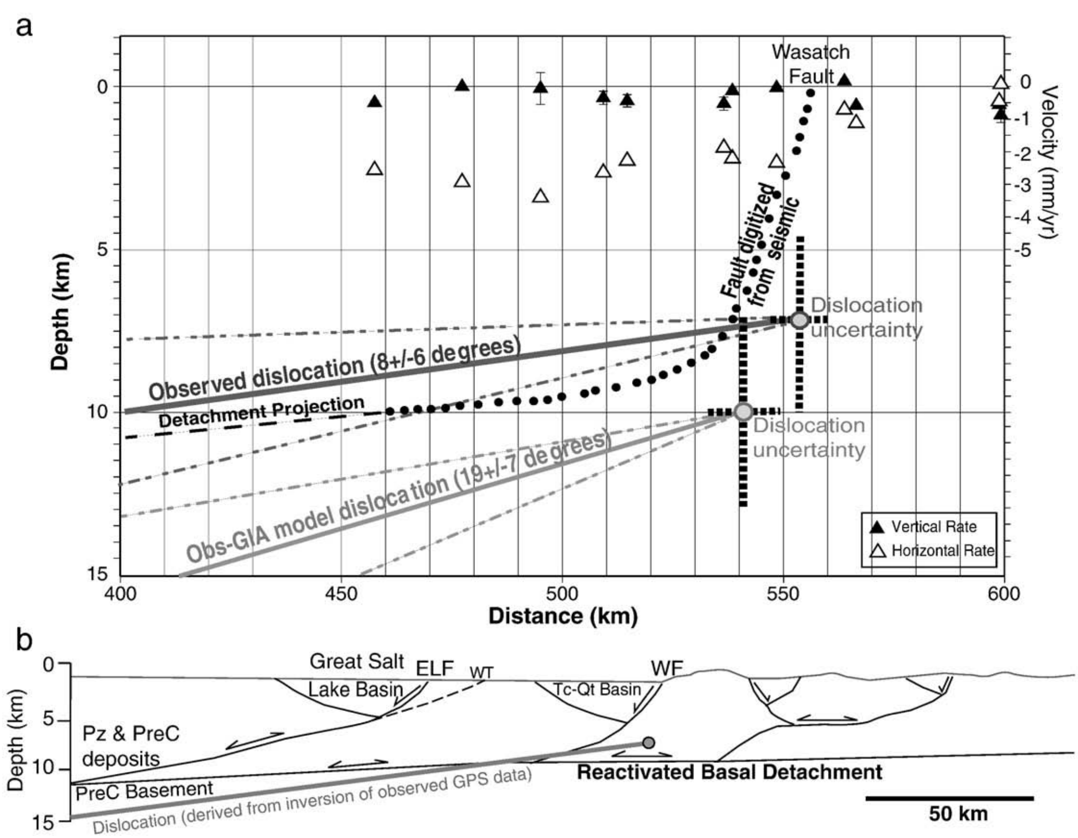

Fig. 8. Schematic cross-sections of the eastern Basin and Range: (a.) showing the location of the Wasatch fault, digitized from the seismic, the horizontal and vertical velocities from continuous GPS data (triangles), and elastic dislocation model results for the observed GPS data (dark gray line) with uncertainties (dashed) and for the observed minus the SNARF GIA model contribution (light gray line) with uncertainties (dashed); and (b.) showing interpretation of the seismic data, dislocation estimated from the observed GPS data, and additional interpretation modified from Constenius (1996).

Andersonian theory, leading to the suggestion that faults form at high angles but are subsequently rotated to lower angles and become inactive, either due to rotation during later episodes of normal faulting along new, steeply dipping structures (Proffett, 1977), or due to isostatic adjustments (Wernicke and Axen, 1988). Thermochronological and paleomagnetic data (e.g., Garcés and Gee, 2007), on the other hand, support active slip on low-angle faults. Thus, revisions to Andersonian theory have been suggested. Some proposed mechanical theories call for rotations of stress due to either lower crustal flow, involving a change in rheology between the elastic upper crust and the viscous lower crust (Lister and Davis, 1989; Melosh, 1990), or resulting from the action of sub-horizontal shear stress at the base of the brittle upper crust (Yin, 1989; Westaway, 1999). Many low-angle normal faults are thought to have evolved from ductile shear zones into brittle faults as removal of the insulating hanging walls cooled the footwall shear zones (Davis and Coney, 1979). However, although these types of faults are thought to record shear-zone evolution in the brittle–ductile transition zone, low-angle normal faults may also play a critical role in the evolution and dynamics of the brittle part of the crust (Axen et al., 2001). In some instances, low-angle normal faults reactivate preexisting low-angle structures. Other hypotheses were proposed, as well, which include high pore-fluid pressure (e.g., Axen, 1992; Reston et al., 2007) and extensional wedge theory (Xiao et al., 1991).

From our model results, the best-fit edge dislocation to the geodetic rate data is a low-angle surface (<30°) at a locking depth of ~7–10 km. This dislocation may be interpreted in several ways. The traditional interpretation of such an elastic dislocation model is that the dislocation plane represents a deeper extension of an upper crustal fault. For our case, we might envision that this deeper portion of the fault represents a reactivated Sevier-age décollement. However, the tip of our model dislocation uniquely specifies only the locus of strain accumulation, and does not dictate the manner by which this elastic strain is converted into fault slip within brittle crustal levels. Thus, a more general interpretation could be that this tip marks an "S-point" in the sense of Willett et al. (1993), indicating the onset of mechanical decoupling that could be facilitated by any number of mechanisms, including aseismic fault slip, localized ductile shear, or crustal flow. Regardless of these possible interpretations, the spatial coincidence of our geodetically inferred dislocation tip with the seismically imaged upper crustal fault structures at or near the brittle–ductile transition strongly suggests a mechanical relationship between upper crustal and lower crustal processes. We do not address the important question of whether or not the dislocation tip dictates the location of the faults (through stress trajectories), or conversely whether the location of the existing faults dictates the location of the tip. Moreover, our data provide no observational basis for claiming that the spatial relationship between the dislocation tip and the upper crustal faults of the eastern Basin and Range remains constant over time. However, it seems safe to assume that the theory of elastic strain accumulation and release would suggest that ephemeral elastic strain represented by the dislocation is ultimately released as permanent strain partitioned among the mapped surface faults over time-scales that are long relative to the nominal earthquake cycle.

The more specific interpretation of the sub-horizontal dislocation as representing a zone of upper and lower crustal detachment might be consistent with previously proposed mechanisms for reconciling Andersonian fault theory with slip on low-angle surfaces. These mechanisms call for rotations of principal stress directions with depth due to either lower crustal flow (Lister and Davis, 1989; Melosh, 1990), or resulting from the action of localized shear zones at the base of the brittle upper crust (Yin, 1989; Holbrook et al., 1991; Westaway, 1999). The dislocation tip may also represent the chloritic breccia zone of Axen (1992), which was proposed to explain slip of low-angle structures via fault weakness due to high pore-fluid pressure and anisotropy imparted by the older mylonitic foliation.

Our seismic data analysis, concentrated on the brittle part of the continental crust, gives us a better understanding of the elastic behavior of the upper crust and how this permanent deformation is distributed. In contrast, our geodetic data measure strain localization at the surface, which can be used to infer strain at or near the brittle–ductile transition. The combination of both datasets helps reconcile lower crustal phenomena that could have implications for active low-angle normal faults (e.g., Wernicke, 1995) and shallower structures above.

A western extrapolation of the low-angle surface that we imaged using seismic and geodetic data might provide a candidate surface across which the intracontinental strain transient described by Davis et al. (2006) could have occurred. The strain transient was recorded by continuous GPS stations located within eastern and central Nevada. It has a similar character to slow slip events recorded in Cascadia, suggesting a subcontinental-scale "megadetachment" near the Moho beneath the Basin and Range (Wernicke et al., 2008). Based on our models and interpretation, if we assume that the low-angle surface is a continuous structure, it would intercept Moho depths (~30 km) at approximately 200 km west of its starting location, in general agreement with the location of the eastern boundary of this "megadetachment". The interaction between these tectonic elements could potentially control the energy transfer across the entire crust within this deformation zone, providing a kinematic basis for understanding lithospheric dynamics across the Basin and Range Province.

6. Conclusions

Subsurface structure derived from seismic reflection data and crustal deformation from using jointly horizontal and vertical geodetic measurements provide new insights to how strain may be accommodated in the upper crust of eastern Basin and Range. We developed a new model for crustal structure and kinematics based on seismic reflection evidence for subsurface fault geometries in central Utah at the Wasatch fault zone and a continuous twelve-year record of GPS measurements that show present-day strain accumulation in the eastern Basin and Range Province. Our GPS modeling results combined with fault geometries derived from seismic reflection data are consistent with a regionally extensive low-angle basal detachment beneath the eastern Basin and Range at depths between 7 and 10 km. Our data support the conclusion that the shallower listric normal faults observed on the seismic data are reactivated Sevier-age structures that accommodate present-day extension of the eastern Basin and Range. These structures may be connected at depth with a regionally extensive low-angle surface, thought to be accommodating aseismic slip at or above the brittle–ductile transition or ductile flow beneath the brittle–ductile transition zone under the present-day Basin and Range extensional regime.

Acknowledgements

We thank: Kiriaki Xiluri and Steve Sorensen for their invaluable help with seismic data loading and computer software maintenance; Lynn Peyton, Kurt Constenius, and Noah Fay for their constructive comments; Bob Krantz, ConocoPhillips, for the valuable discussions. We also like to thank our reviewers, Laura Serpa and Bill Hammond, for their helpful and constructive comments. We used data from the PBO and PBO NUCLEUS component of the NSF Earthscope facility operated by UNAVCO. The CGPS stations used were conceived, constructed, operated, and maintained through the efforts of numerous NSF investigators and UNAVCO Facility engineers. Industry seismic data were donated by Amoco Production Company (BP) and ExxonMobil. Seismic data were processed using Promax software (Landmark Graphics Inc.) and interpreted using The Kingdom Suite from Seismic Micro-Technologies. Mark Brandon provided a software implementation of the constrained random search algorithm. This

Please cite this article as: Velasco, M.S., et al., Subsurface fault geometries and crustal extension in the eastern Basin and Range Province, western U.S., Tectonophysics (2009), doi:10.1016/j.tecto.2009.05.010

project was supported in part by NSF Tectonics grant 0510484 to R.A. Bennett.

References

Abers, G.A., 1991. Possible seismogenic shallow-dipping normal faults in the Woodlark-D'Entrecasteaux extensional province, Papua New Guinea. Geology 19 (12), 1205–1208.

Allmendinger, R.W., Sharp, J.W., Von Tish, D., Serpa, L., Brown, L., Kaufmann, S., Oliver, J., Smith, R.B., 1983. Cenozoic and Mesozoic structure of the eastern Basin and Range Province, Utah, from COCORP seismic-reflection data. Geology 11, 532–536.

Anders, M.H., Christie-Blick, N., 1994. Is the Sevier Desert reflection of west-central Utah a normal fault? Geology 22, 771–774.

Anderson, R.E., 1971. Thin-skin distension in Tertiary rocks of southwestern Nevada. Geological Society of America Bulletin 82, 43–58.

Armstrong, R.L., 1972. Low-angle (denudation faults), hinterland of the Sevier orogenic belt, eastern Nevada and western Utah. Geological Society of America Bulletin 83, 1729–1754.

Axen, G.J., 1992. Pore pressure, stress increase, and fault weakening in low-angle normal faulting. Journal of Geophysical Research 97 (B6), 8979–8991.

Axen, G.J., Selverstone, J., Wawrzyniec, T., 2001. High-temperature embrittlement of extensional Alpine mylonite zones in the midcrustal ductile–brittle transition. Journal of Geophysical Research 106, 4337–4348.

Bennett, R.A., Wernicke, B.P., Davis, J.L., 1998. Contiuous GPS measurements of contemporary deformation across the northern Basin and Range. Geophysical Research Letters 25, 563–566.

Bennett, R., Wernicke, B., Niemi, N., Friedrich, A., Davis, J., 2003. Contemporary strain rates in the northern Basin and Range province from GPS data. Tectonics 22 (2), 1008.

Bennett, R., Hreinsdóttir, S., Velasco, M.S., Fay, N., 2007. GPS constraints on vertical crustal motion in the northern Basin and Range. Geophysical Research Letters 34, L22319.

Black, B.D., Lund, W.R., Schartz, D.P., Gill, H.E., Mayes, B.H., 1996. Paleoseismology of Utah, Volume 7—Paleoseismic Investigation on the Salt Lake City Segment of the Wasatch Fault Zone at the South Fork Dry Creek and Dry Gulch Sites, Salt Lake County, Utah: Utah Geological Survey Special Study, vol. 92, p. 22.

Blewitt, G., Lavallee, D., 2002. Effect of annual signals on geodetic velocity. Journal of Geophysical Research 107 (B7).

Blewitt, G., Argus, D., Bennett, R., Bock, Y., Calais, E., Craymer, M., Davis, J., Dixon, T., Freymueller, J., Herring, T., Johnson, D., Larson, K., Miller, M., Sella, G., Snay, R., Tamisiea, M., 2005. A Stable North American Reference Frame (SNARF): First Release, Proceedings of the Joint UNAVCO/IRIS Workshop, Stevenson, WA, USA, June 9–11.

Brachetti, P., De Felice Ciccoli, M., Di Pillo, G., Lucidi, S., 1997. A new version of the Prices algorithm for global optimization. Journal of Global Optimization 10, 165–184.

Brock, W.G., Engelder, T., 1977. Deformation associated with the movement of the Muddy Mountain overthrust in the Buffington window, southeastern Nevada. Geological Society of America bulletin 88, 1667–1677.

Byerlee, J., 1978. Friction of rocks. Pure and Applied Geophysics 116, 615–626.

Caskey, S.J., Wesnousky, S.G., Zhang, P., Slemmons, D.B., 1996. Surface faulting of the 1954 Fairview Peak (MS 7.2) and Dixie Valley (MS 6.8) earthquakes, central Nevada. Bulletin of the Seismological Society of America 86, 761–787.

Chang, W., Smith, R., Meertens, M., Harris, R., 2006. Contemporary deformation of the Wasatch Fault, Utah, from GPS measurements with implications for interseismic fault behavior and earthquake hazard: observations and kinematic analysis. Journal of Geophysical Research 111 (B11), 405.

Colman, S., Kelts, K., Dinter, D., 2002. Depositional History and Neotectonics in Great Salt Lake, Utah, from High-resolution Seismic Stratigraphy, vol. 148, pp. 61–78.

Coogan, J.C., DeCelles, P.G., 1996. Seismic architecture of the Sevier Desert detachment basin: evidence for large-scale regional extension. Geology 24, 933–936.

Coney, P.J., Harms, T.A., 1984. Cordilleran metamorphic core complexes: Cenozoic extensional relics of Mesozoic compression. Geology 12, 550–554.

Constenius, K., 1996. Late Paleogene extensional collapse of the Cordilleran foreland fold and thrust belt. Geological Society of America bulletin 108, 20–39.

Constenius, K., Esser, R., Layer, P., 2003. Extensional collapse of the Charleston-Nebo Salient and its relationship to space–time variations in Cordilleran orogenic belt tectonism and continental stratigraphy. In: Raynolds, R., Flores, R. (Eds.), Cenozoic Systems of the Rocky Mountains Region. Rocky Mountain SEPM, Denver, CO.

Crittenden, M.D., Coney, P.J., Davis, G.H., 1980. Cordilleran metamorphic core complexes. Geological Society of America Memoir 153, 490.

Davis, G.H., Coney, P.J., 1979. Geologic development of Cordilleran metamorphic core complexes. Geology 7, 120–124.

Davis, J.L., Wernicke, B.L., Bisnath, S., Neimi, N.A., Elosegui, P., 2006. Subcontinental-scale crustal velocity changes along the Pacific-North America transform plate boundary from BARGEN GPS data. Nature 441, 1131. doi:10.1038/nature0478112/2006.

DeCelles, P.G., Coogan, J.C., 2006. Regional structure and kinematic history of the Sevier fold-and-thrust belt, central Utah. Geological Society of America Bulletin 118, 841–864.

Dickinson, W., 2002. The Basin and Range Province as a composite extensional domain. International Geology Review 44, 1–38.

Dixon, T.H., Miller, M., Farina, F., Wang, H., Johnson, D., 2000. Present-day motion of the Sierra Nevada block and some tectonic. implications for the Basin and Range province, North America Cordillera. Tectonics 19, 1–24.

Doser, D.I., Smith, R.B., 1989. An assessment of source parameters of earthquakes in the cordillera of the western United States. Bulletin of the Seismological Society of America 79, 1383–1409.

Eaton, G., 1982. The Basin and Range Province: origin and tectonic significance. Annual Review of Earth and Planetary Sciences 10, 409–440.

Friedrich, A., Wernicke, B., Niemi, N., 2003. Comparison of geodetic and geologic data from the Wasatch region, Utah, and implications for the spectral character of Earth deformation at periods of 10 to 10 million years. Journal of Geophysical Research 108 (B4), 2199.

Friedrich, A.M., Lee, J., Wernicke, B.P., Sieh, K., 2004. Geologic context of geodetic data across a Basin and Range normal fault, Crescent Valley, Nevada. Tectonics 23, TC2015.

Garcés, M., Gee, J.S., 2007. Paleomagnetic evidence of large footwall rotations associated with low-angle normal faults at the Mid-Atlantic Ridge. Geology 35, 279–282.

Gilbert, H., Sheehan, A., 2004. Images of crustal variations in the intermountain west. Journal of Geophysical Research 109, B03306.

Hamilton, W.B., 1978. Mesozoic tectonics of the western United States. Soc. Econ. Paleontol. Mineral., Pacific Sec., Paleogeography Symposium, vol. 2, pp. 33–70.

Hammond, W.C., Thatcher, W., 2004. Contemporary tectonic deformation of the Basin and Range province, western United States: 10 years of observation with the Global Positioning System. Journal of Geophysical Research 109, B08403.

Harris, R.A., Smith, R.B., Chang, W.L., Meertens, C.M., Friedrich, A.M., 2000. Temporal distribution of extensional strain across the southern Wasatch fault zone: geological constraints for the GPS velocity field. Transactions — American Geophysical Union, EOS 81, F1230.

Herring, T.A., King, R.W., McClusky, S.C. (2006a). GAMIT Reference Manual GPS Analysis at MIT Release 10.3. Department of Earth, Atmospheric, and Planetary Sciences Massachussetts Institute of Technology.

Herring, T.A., King, R.W., McClusky, S.C. (2006b). Global Kalman Filter VLBI and GPS Analysis Program Release 10.3. Department of Earth, Atmospheric, and Planetary Sciences Massachussetts Institute of Technology.

Holbrook, W.E., Catchings, R.D., Jarchow, C.M., 1991. Origin of deep crustal reflections: implications of coincident seismic refraction and reflection data in Nevada. Geology 19, 175–179.

Horton, B.K., Constenius, K.N., DeCelles, P.G., 2004. Tectonic control on coarse-grained foreland-basin sequences; an example from the Cordilleran foreland basin, Utah. Geology 32 (7), 637–640.

Johnson, R.A., Loy, K.L., 1992. Seismic reflection evidence for seismogenic low-angle faulting in southeastern Arizona. Geology 20, 597–600.

Jones, A., Gough, D., Kurtz, R., DeLaurier, J., Boerner, D., Craven, J., Ellis, R., Mc-Neice, G., 1992. Electromagnetic images of regional structure in the southern Canadian Cordillera. Geophysical Research Letters 12, 2373–2376.

Lister, G.S., Davis, G.A., 1989. The origin of metamorphic core complexes and detachment faults formed during Tertiary continental extension in the northern Colorado River region, U.S.A. Journal of Structural Geology 11, 65–94.

Lund, W.R., Black, B.D., 1998. Paleoseismology of Utah, Volume 8—Paleoseismic Investigation at Rock Canyon, Provo Segment, Wasatch Fault Zone, Utah County, Utah: Utah Geological Survey Special Study, vol. 93, p. 21.

Malservisi, R., Dixon, T., LaFemina, P., 2003. Holocene slip rate of the Wasatch fault zone, Utah, from geodetic data. Geophysical Research Letters 30, 1673.

Martinez, L.J., Meertens, C.M., Smith, R.B., 1998. Rapid deformation rates along the Wasatch fault zone, Utah, from first GPS measurements with implications for earthquake hazard. Geophysical Research Letters 25 (4), 567–570.

McCalpin, J.P., Nelson, C., 2001. Long recurrence records from the Wasatch fault, Utah, USGS NEHRP Annual Report, Grant No. 99HQGR0058, p. 61.

McCalpin, J.P., Forman, S.L., Lowe, M., 1994. Reevaluation of Holocene faulting at the Kaysville site, Weber segment of the Wasatch fault zone, Utah. Tectonics 13 (1), 1–16.

Melosh, H., 1990. Mechanical basis for low-angle normal faulting in the Basin and Range province. Journal of Nature 343, 331–335.

Mohapatra, G.K., Petropoulos, G., Johnson, R.A., 1993. Extension and structural evolution beneath the Great Salt Lake, Utah: Results from reflection seismic imaging: EOS, Transactions, American Geophysical Union, vol. 74 (supplement), p. 412.

Mohapatra, G.K. (1996). Faulting and basin geometry beneath the Great Salt Lake: implications for basin evolution and Cenozoic extension. Unpublished PhD Dissertation, Department of Geosciences, University of Arizona, Tucson, Arizona, 1–159.

Mohapatra, G.K., Johnson, R.A., 1998. Localization of listric faults at thrust ramps beneath the Great Salt Lake Basin, Utah: evidence from seismic imaging and finite element modeling. Journal of Geophysical Research 103 (B5), 10,047–10,063.

Mohapatra, G.K., Petropoulos, G., Johnson, R.A., 1993. Extension and structural evolution beneath the Great Salt Lake, Utah: results from reflection seismic imaging. Transactions — American Geophysical Union, EOS 74, 412 (supplement).

Niemi, N., Wernicke, B., Frederick, A., Simmons, M., Bennett, R., Davis, J., 2004. BARGEN continuous GPS data across the eastern Basin and Range province, and implications for fault system. Geophysical Journal International 159 (3), 842–862.

Otton, J., 1995. Western frontal fault of the Canyon Range: is it the breakaway zone of the Sevier Desert detachment. Geology 23 (6), 547–550.

Press, W.H., Flannery, B.P., Teukolsky, S.A., Vetterling, W.T., 1986. Numerical Recipes. Cambridge University Press, London.

Proffett Jr., J.M., 1977. Cenozoic geology of the Yerington District, Nevada, and implications for nature and origin of Basin and Range faulting. Geological Society of America Bulletin 88, 247–266.

Reston, T.J., Leythaeuser, T., Booth-Rea, G., Sawyer, D., Klaeschen, D., Long, C., 2007. Movement along a low-angle normal fault: the S reflector west of Spain. Geochemistry Geophysics Geosystems 8, Q06002.

Savage, J.C., 1983. A dislocation model for strain accumulation and release at a subduction zone. Journal of Geophysical Research 88, 4984–4996.

Savage, J.C., 1990. Equivalent strike-slip cycles in half-space and lithosphere–asthenosphere earth models. Journal of Geophysical Research 95, 4873–4879.

Savage, J.C., 2000. Viscoelastic-coupling model for the earthquake cycle driven from below. Journal of Geophysical Research-Solid Earth 105, 25,525–25,532.

Savage, J.C., Lisowski, M., Prescott, W.H., 1992. Strain accumulation across the Wasatch fault near Ogden, Utah. Journal of Geophysical Research 97 (B2), 2071–2083.

Please cite this article as: Velasco, M.S., et al., Subsurface fault geometries and crustal extension in the eastern Basin and Range Province, western U.S., Tectonophysics (2009), doi:10.1016/j.tecto.2009.05.010

Savage, J.C., Svarc, J.L., Prescott, W.H., 1999. Geodetic estimates of fault slip rates in the San Francisco Bay Area. Journal of Geophysical Research 104, 4995–5002.
Scholz, C.H., 1990. The Mechanics of Earthquakes and Faulting, 1st ed. Cambridge Univ. Press, Cambridge.
Schwartz, D.P., Coppersmith, K.J., 1984. Fault behavior and characteristic earthquakes: examples from Wasatch and San Andreas fault zones. Journal of Geophysical Research 89, 5681–5698.
Shimazaki, K., Nakata, T., 1980. Time-predictable recurrence model for large earthquakes. Geophysical Research Letters 7, 279–282.
Sibson, R.H., 1985. A note on fault reactivation. Journal of Structural Geology 7, 751–754.
Smith, R.B., Sbar, M., 1974. Contemporary tectonics and seismicity of the western United States with emphasis on the Intermountain Seismic Belt. Bulletin of the Geological Society of America 85, 1205–1218.
Smith, R.B., Bruhn, R.L., 1984. Intraplate extensional tectonics of the western U.S. Cordillera — inferences on structural style from seismic-reflection data, regional tectonics and thermal–mechanical models of brittle–ductile deformation. Journal of Geophysical Research 89 (B7), 5733–5762.
Smith, R.B., Arabasz, W.J., 1991. Seismicity of the Intermountain Seismic Belt, in Neotectonics of North America. In: Slemmons, D.B., Engdahl, E.R., Zoback, M.L., Blackwell, D.D. (Eds.), Geol. Soc. Am., SMV V-1, Decade Map, vol. 1, pp. 185–228.
Spencer, J., 1984. Role of tectonic denudation in warping and uplift of low-angle normal faults. Geology 12, 95–98.
Spencer, J.E., Chase, C.G., 1989. Role of crustal flexure in initiation of low-angle normal faults and implications for structural evolution of the Basin and Range province. Journal of Geophysical Research 94, 1765–1775.
Stewart, J.H., 1978. Basin-range structure in western North America: a review. In: Smith, R.B., Eaton, G.P. (Eds.), Cenozoic Tectonics and Regional Geophysics of the Western Cordillera: Mem. Geol. Soc. Am., vol. 152, pp. 1–31.
Satarugsa, P., Johnson, R.A., 1998. Crustal velocity structure beneath the eastern flank of the Ruby Mountains metamorphic core complex: results from normal-incidence to wide-angle seismic data. Tectonophysics 295 (3), 369–395 (27).
Thatcher, W., Foulger, G.R., Julian, B.R., Svarc, J., Quilty, E., Bawden, G.W., 1999. Present-day deformation across the Basin and Range Province, western United States. Science 283 (5408), 1714–1718.
Vergne, J., Cattin, R., Avouac, J.P., 2001. On the use of dislocations to model interseismic strain and stress build-up at intracontinental thrust faults. Geophysical Journal International 147, 155–162.
Von Tish, D.B., Allmendinger, R.W., Sharp, J.W., 1985. History of Cenozoic extension in central Sevier Desert, west-central Utah, from COCORP seismic reflection data. American Association of Petroleum Geologists Bulletin 69, 1077–1087.
Wallace, R.E., 1987. Grouping and migration of surface faulting and variations in slip rates on faults in the Great Basin province. Seismological Society of America Bulletin 77 (3), 868–876.
Wernicke, B., 1981. Low-angle normal faults in the Basin and Range Province: Nappe tectonics in an extending orogen. Nature 291, 645–648.
Wernicke, B., 1995. Low-angle normal faults and seismicity: a review. Journal of Geophysical Research 100, 20,159–20,174.
Wernicke, B., Axen, G.J., 1988. On the role of isostasy in the evolution of normal fault systems. Geology 16, 848–851.
Wernicke, B., Axen, G.J., Snow, J.K., 1988. Basin and Range extensional tectonics at the latitude of Las Vegas, Nevada. Geological Society of America Bulletin 100, 1738–1757.
Wernicke, B., Davis, J.L., Bennett, R.A., Normandeau, J.E., Friedrich, A.M., Niemi, N.A., 2004. Tectonic implications of a dense continuous GPS velocity field at Yucca Mountain, Nevada: testing the extensional detachment paradigm: scientific drilling in the Sevier Desert basin. Journal of Geophysical Research 109 (B12404).
Wernicke, B., Davis, J.L., Niemi, N.A., Luffi, P., Bisnath, S., 2008. Active megadetachment beneath the western United States. Journal of Geophysical Research 113, B11409. doi:10.1029/2007JB005375.
Westaway, R., 1999. The mechanical feasibility of low-angle normal faulting. Tectonophysics 308, 407–443.
Wheeler, R.L., Krystinik, K.B., 1992. Persistent and nonpersistent segmentation of the Wasatch Fault Zone, Utah: statistical analysis for evaluation of seismic hazard. In: Gori, P.L., Hays, W.W. (Eds.), Assessment of Regional Earthquake Hazards and Risk along the Wasatch Front, Utah: U.S. Geol. Surv. Profess. Pap. 1500-A-J, pp. B1–B47.
Willett, R.L., Ruel, R.R., West, K.W., Pfeiffer, L.N., 1993. Experimental demonstration of a Fermi surface at one-half filling of the lowest Landau level. Physical Review Letters 71, 3846–3849.
Wills, S., Anders, M.H., 1996. Western frontal fault of the Canyon Range: is of the Sevier Desert detachment?: Comment. Geology 24, 667–668.
Wilson, P.N., Presnell, R.D., 1992. Alteration, mineral deposits and structural relationships of the Oquirrh Mountains, Utah. In: Wilson, J.R. (Ed.), Field Guide to Geologic Excursions in Utah and Adjacent Areas of Nevada, Idaho and Wyoming: Utah Geological Survey, p. 481.
Wright, L.A., Troxel, B.W., 1973. Shallow-fault interpretation of Basin and Range structure, southwestern Great Basin. In: de Jong, K.A., Scholten, R. (Eds.), Gravity and Tectonics. John Wiley and Sons, New York, pp. 397–407.
Xiao, H., Dahlen, F.A., Suppe, J., 1991. Mechanics of extensional wedges. Journal of Geophysical Research 96, 10301–10318.
Yin, A., 1989. Origin of regional rooted low-angle normal faults: a mechanical model and its implications. Tectonics 8, 469–482.
Zatman, S., 2000. On steady rate coupling between an elastic upper crust and a viscous interior. Geophysical Research Letters 27, 2421–2424.

Please cite this article as: Velasco, M.S., et al., Subsurface fault geometries and crustal extension in the eastern Basin and Range Province, western U.S., Tectonophysics (2009), doi:10.1016/j.tecto.2009.05.010